

Spin polarized proton beam generation from gas-jet targets by intense laser pulses

Luling Jin,¹ Meng Wen,^{1,*} Xiaomei Zhang,^{2,†} Anna Hützen,^{3,4}
Johannes Thomas,⁵ Markus Büscher,^{3,4} and Baifei Shen^{2,6}

¹*Department of Physics, Hubei University, Wuhan 430062, China*

²*State Key Laboratory of High Field Laser Physics,
Shanghai Institute of Optics and Fine Mechanics,
Chinese Academy of Sciences, Shanghai 201800, China*

³*Peter Grünberg Institut (PGI-6), Forschungszentrum Jülich, Wilhelm-Johnen-Str. 1, 52425 Jülich, Germany*

⁴*Institut für Laser- und Plasmaphysik, Heinrich-Heine-Universität Düsseldorf, Universitätsstr. 1, 40225 Düsseldorf, Germany*

⁵*Institut für Theoretische Physik I, Heinrich-Heine-Universität Düsseldorf, Universitätsstr. 1, 40225 Düsseldorf, Germany*

⁶*Department of Physics, Shanghai Normal University, Shanghai 200234, China*

(Dated: August 6, 2022)

A method of generating spin polarized proton beams from a gas jet by using a multi-petawatt laser is put forward. With currently available techniques of producing pre-polarized monatomic gases from photodissociated hydrogen halide molecules and petawatt lasers, proton beams with energy $\gtrsim 50$ MeV and $\sim 80\%$ polarization are proved to be obtained. Two-stage acceleration and spin dynamics of protons are investigated theoretically and by means of fully self-consistent three dimensional particle-in-cell simulations. Our results predict the dependence of the beam polarization on the intensity of the driving laser pulse. Generation of bright energetic polarized proton beams would open a domain of polarization studies with laser driven accelerators, and have potential application to enable effective detection in explorations of quantum chromodynamics.

The polarization of a beam describes the collective spin state for an ensemble of particles. The generation of such polarized particle beams is a topic of great interest in accelerator physics, since it plays important roles in solving a wide variety of scientific and medical problems [1, 2]. In particular, spin polarized proton beams enable key measurements in explorations of the quantum-chromodynamics landscape [3, 4]. High luminosity is required in such experiments for both high energy colliders to solve the outstanding proton spin puzzle [5, 6] and low energy colliders to extend Standard Model tests [7]. However, the intensity of the polarized beams is generally limited to several hundred milliamperes [8], which is very difficult to be further increased at a traditional accelerator [9]. Proton beams of much higher intensity ($\gtrsim 1$ kiloampere) are obtained with laser driven accelerators. Therefore, investigation of spin effects of protons in laser accelerators becomes timely and interesting, because it enables new low-cost, compact laser accelerators of polarized proton beams.

With the advent of ultra-intense lasers up to ~ 10 PW [10–12], plasma accelerators are now capable of providing beams with energies of almost hundred MeV per unit charge [13–18]. At such high laser intensities spin effects are expected to occur which would open a wide domain of polarization studies [19–25]. There have been multiple theoretical works how to generate polarized beams in laser driven accelerators [26–31]. These show that underdense plasmas provide an unique opportunity for generation of polarized beams already at existing laser facilities, thanks to recent experimental progress of producing polarized atomic hydrogen gases with densities above 10^{19} cm^{-3} [32]. Although such prepolarized gases

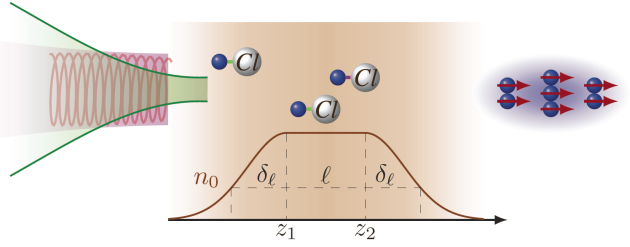


FIG. 1. A schematic diagram showing laser acceleration of polarized protons from a dense hydrogen chloride gas target (brown), see also a related experimental setup in [26]. Molecules are initially aligned along z -axis via a weak optical laser. Blue and white balls represent nuclei of hydrogen and chlorine atoms, respectively. Before the acceleration driven by an intense laser beam (indicated by the green area), a weak circularly polarized UV laser (purple area) is used to generate the polarized atoms along the longitudinal direction via molecular photodissociation. The brown curve indicates the initial density distribution of the gas-jet target. The polarized proton beam is shown on the right (blue) with arrows (red) presenting the polarization direction.

can be used in principle to produce multi-MeV proton beams [33–37], an intuitive and optimized acceleration regime and a comprehensive understanding of the acceleration mechanisms is still pending.

In this Letter, we report the first three dimensional (3D) Particle-In-Cell (PIC) simulation result of laser driven spin motion of protons in pre-polarized gases. Our approach of manipulating spin properties of beams complements the well developed schemes for conventional accelerators as polarized proton sources. The schematic diagram is shown in Fig. 1. The laser system comprises a weak circularly polarized UV laser to generate spin po-

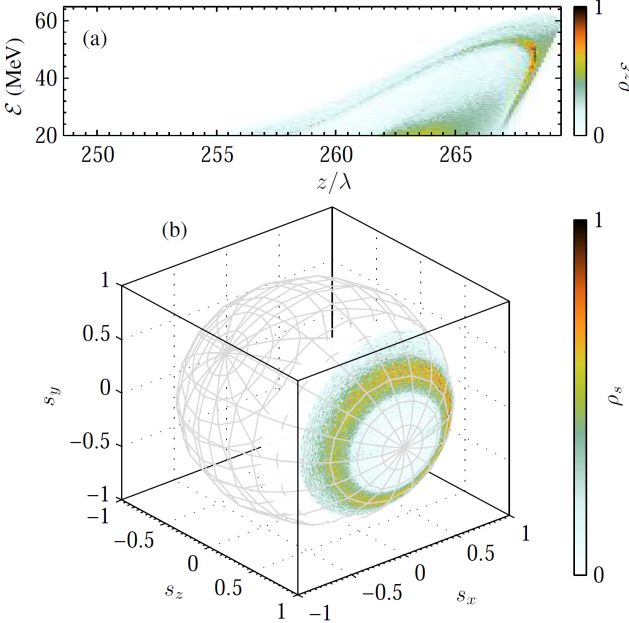


FIG. 2. Snapshots at $t = 330\lambda/c$ of: (a) phase-space distribution, and (b) spin spread of protons with energy $\mathcal{E} \geq 20$ MeV on the Bloch sphere. Simulation parameters can be found in the text.

larized atoms via photodissociation, and an intense laser to accelerate protons. The accelerated proton beam can be depolarized via asynchronous spin precession in inhomogeneous electromagnetic fields of laser driven plasmas. Using a gaseous HCl target with molecular density $\sim 10^{19} \text{ cm}^{-3}$ and a 1.3 petawatt (PW) laser as an example, the energy of accelerated polarized protons can be as high as 50 MeV, with a beam polarization above 80 %. The corresponding phase space distribution and the spin spread of accelerated protons are shown in Fig. 2. As will be seen below, the energy increases with the power of the driving laser, while the polarization of the beam is almost preserved.

For the success of laser induced spin-polarized beam acceleration, several criteria have to be satisfied. First, the parameters assumed in the simulations can be realized in experiments. Second, protons are accelerated effectively in the setup with a polarized/polarizable target. Third, a high degree of polarization of the accelerated protons is retained. The first criterion is met by adopting currently available PW lasers and a gas jet of polarized atoms with hydrogen density $\sim 10^{19} \text{ cm}^{-3}$. The polarization of the gas can be built via laser photodissociation with circularly polarized UV laser pulses (see Fig. 1) [32]. After the molecules are dissociated to polarized atoms, the polarization is transferred from electrons to nuclei within a few 100 ps and oscillates between electrons and nuclei afterwards. Experiments should be designed such that the polarized gas is fully ionized by the PW laser when the hydrogen nuclei acquire a high degree of polar-

ization. The delay between the UV laser and the driving pulse for ion acceleration should therefore be carefully controlled, which is accessible by splitting one laser beam [29] or by combining different laser systems [26]. The remaining two criteria of efficient proton acceleration and small spin smearing require the laser beam to pile up large number of electrons but stimulate weak magnetic fields. Both of these two conditions will be demonstrated below with full 3D-PIC simulations. Since protons are heavier than electrons, their spin precession is roughly three orders of magnitude slower. On the other hand, the longer interaction times and the necessarily stronger fields for ion acceleration can inevitably induce significant precession depolarization of the accelerated proton beams.

Acceleration and spin precession of protons are investigated via 3D-PIC simulations, employing the EPOCH code [38] which has been extended by spin effects [22]. In the Bloch sphere presentation, an arbitrary spin state $c_1 |\uparrow\rangle + c_2 |\downarrow\rangle$ can be represented by the unit spin vector $\mathbf{s} = (c_1^* c_2 + c_1 c_2^*, i c_1 c_2^* - i c_1^* c_2, |c_1|^2 - |c_2|^2)$, where $|\uparrow\rangle$ denotes a spin direction parallel to the z -axis. In PIC simulations, the classical spin of a charged particle with kinetic momentum \mathbf{p} and velocity \mathbf{v} is characterized by the unit vector \mathbf{s} , which corresponds to one point on the sphere of Fig. 2(b). Furthermore, the Landau-Lifshitz equation $d\mathbf{p}/dt = \mathbf{F}_L + \mathbf{F}_R$ was applied to calculate the motion of electrons in the radiation-dominated regime driven by PW lasers [39]. Here $\mathbf{F}_L = -q(\mathbf{E} + \mathbf{v} \times \mathbf{B})$ is the Lorentz force and $\mathbf{F}_R \approx q^4/(6\pi\epsilon_0 m^2 c^5)[(\mathbf{v} \cdot \mathbf{E}/c)^2 - (\mathbf{E} + \mathbf{v} \times \mathbf{B})^2]\gamma^2 \mathbf{v}$ is the Landau-Lifshitz force, with γ the relativistic Lorentz factor, c the speed of light in vacuum, m and q the electron mass and charge, respectively.

The 3D-PIC simulations are performed with a moving box of size $100\lambda \times 80\lambda \times 80\lambda$ represented by a $1000 \times 400 \times 400$ grid at speed of light c and a total pseudoparticle number of 8×10^8 . The laser pulse for proton acceleration (green area in Fig. 1) with a bi-Gaussian envelope $\mathbf{a} = \mathbf{e}_x a_0 \exp[-(t-z/c+z_0/c)^2/T^2-r^2/w_0^2]$ and a focal position z_0 propagates along the z -axis, where the laser amplitude $a_0 = 25$, focal radius $w_0 = 10\lambda$, wavelength $\lambda = 800 \text{ nm}$, and temporal duration $T = 10\lambda/c$. In order to reach a high acceleration efficiency, the laser pulse is focused to the left boundary of the gas target $z_0 = z_1 = 50\lambda$. The target is assumed to be a fully ionized plasma of HCl gas, with all protons initially polarized along the z -axis $\langle \mathbf{s} \rangle \cdot \mathbf{e}_z = 1$. Its density profile, as shown by the brown curve in Fig. 1, is a uniform plateau with steep edges [37, 40–42]. The length of the target is $\ell = z_2 - z_1 = 200\lambda$. The density gradient at the edge is expressed as $n = n_0 \exp[-(z - z_i)^2/\delta_\ell^2]$ with $\ell = 5\lambda$, where $i = 1$ and 2 correspond to the left and right boundaries of the target, respectively. In the following simulations, gas jets with density $n_0 = 0.36n_c$ are applied where $n_c = \epsilon_0 m \omega^2 / e^2$ is the critical plasma density, ϵ_0 the vacuum permittivity, and $\omega = 2\pi c/\lambda$

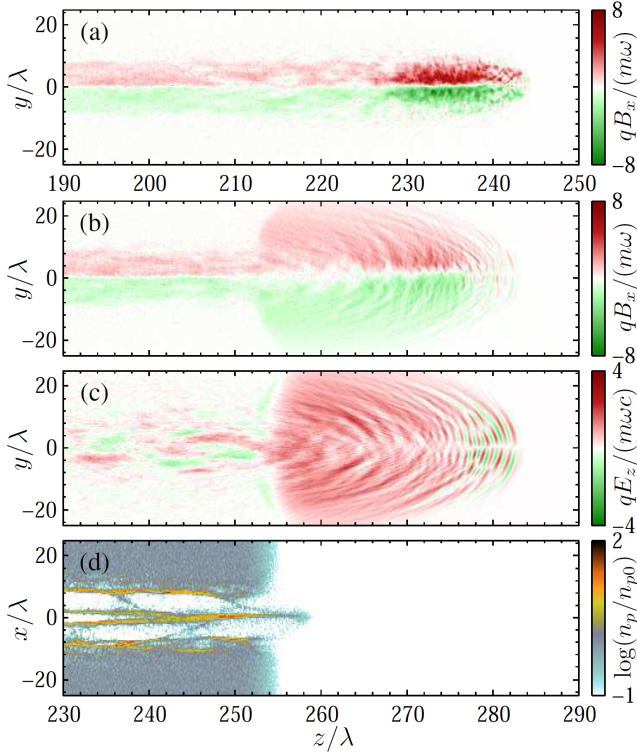


FIG. 3. Snapshots of: (a) azimuthal magnetic field at $t = 250\lambda/c$, and (b) azimuthal magnetic field (c) longitudinal electric field and (d) proton density at $t = 290\lambda/c$.

the laser frequency. One should note that the proton density n_p is lower than the plasma density, i.e., $n_p = n_0/(Z_H + Z_{Cl}) \approx 3.48 \times 10^{19} \text{ cm}^{-3}$, with charge numbers of hydrogen $Z_H = 1$ and chlorine $Z_{Cl} = 17$.

Acceleration of protons and spin precession take place within the plasma channel driven by the intense laser. This channel is formed by ponderomotive expulsion of charge lying within the laser's path, as a relativistic self-focusing effect in high intensity laser plasma interactions when the laser power exceeds the critical value $P_c = 17n_c/n_0$ GW. In this investigation, a much higher power laser pulse propagates in underdense plasma, $P_L = 21.49a_0^2w_0^2/\lambda^2$ GW $\gg P_c$, leading to an additional central electron filament enclosed in the evacuated channel [43, 44]. The displacement of electrons introduces a radial electric field E_r in the plasma channel, as well as an azimuthal magnetic field around the channel axis B_ϕ . The magnetic field B_ϕ is represented in Fig. 3(a) by B_x in the $z - y$ plane. Effected by the space charge field E_r , ions also move into the filament along the channel axis. However, due to the small electron-to-proton mass ratio 1/1836, protons converge towards the center on a longer time scale as compared to the electrons, i.e., the electron filament appears inside the laser fields while the proton filament forms behind the laser pulse. We note that the admixture of chlorine nuclei with even smaller charge-to-mass ratio is advantageous for proton acceler-

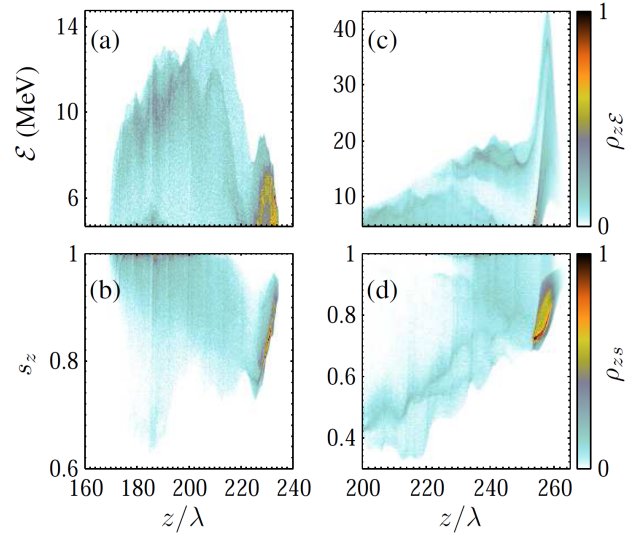


FIG. 4. Distribution of energetic protons (with $\mathcal{E} \geq 5$ MeV) in (a) (c) phase space and (b) (d) space with spin component s_z and z -axis. (a), (b) and (c), (d) corresponds to density plots at $t = 250\lambda/c$ and $t = 290\lambda/c$, respectively.

ations, as has been pointed out already in Ref. [34]. The filament of chlorine nuclei appear behind the proton filament in the plasma channel. Due to the different responds of the particles, a longitudinal space-charge field is formed within the plasma channel. Therefore, protons are accelerated in forward and transverse directions. In addition to the first-stage acceleration in the plasma channel, we find a second effect at the rear end of the gas jet, which significantly enhances the proton energies. Around the sharp rear boundary of the target, transverse expansion of the magnetic field generates a strong longitudinal field which contributes as a secondary acceleration, known as magnetic vortex acceleration [45–47]. When the electrons driven by the laser pulse pass though the rear boundary, the azimuthal magnetic fields expands into the vacuum under large angles. Figures 3(b) and (c) indicates that the transverse expansion of the azimuthal magnetic fields introduces the strong longitudinal electric field $E_z \gtrsim m\omega c/q$ according to the Faraday's law. The focused protons in the filament near the rear boundary are then accelerated strongly as shown in Fig. 3(d).

Figures 4(a) and (b) present effects of the proton acceleration in the plasma channel (with $z < z_2$), and the spin distribution of energetic protons, respectively. It indicates at $t = 250\lambda/c$ many energetic protons start to converge to the front of the proton filament around $z_f = 230\lambda$. The energy of these *front protons* is less than 10 MeV. In contrast to that, the *tail protons*, which converge to the filament before ($t < 250\lambda/c$) and sit on the left side with $z < z_f$, are accelerated further to energies beyond 10 MeV. The spin precession for these front protons and tail protons play different roles as will be discussed below. The PIC simulations have provided clear

evidences for the strong magnetic field in the laser driven plasma channel as shown in Figs. 3(a) and (b). In order to assure that the accelerated protons are not depolarized totally during the convergence to the filament [see Fig. 3(d)], spin precession is calculated in the PIC simulations with the Thomas-Bargmann-Michel-Telegdi equation [48, 49]

$$\frac{ds}{dt} = \frac{q}{Mc} \mathbf{s} \times \left[\left(G + \frac{1}{\gamma} \right) \mathbf{B} - \frac{G\gamma \mathbf{v} \cdot \mathbf{B}}{\gamma + 1} \frac{\mathbf{v}}{c^2} - \left(G + \frac{1}{\gamma + 1} \right) \frac{\mathbf{v}}{c} \times \mathbf{E} \right], \quad (1)$$

where $G \approx 1.79$ is the anomalous magnetic moment of the proton and M is the proton mass. Because of the slow response of the protons, a long time spin precession in the azimuthal magnetic field of the plasma channel enhance the depolarization of pre-polarized protons, while other depolarization effects are negligibly small [31]. Recalling that $\gamma - 1 \ll 1$, the spin of protons in the filament can be roughly estimated via $\mathbf{s} \approx \int_0^T dt (q/Mc) (G + 1) \mathbf{s} \times \mathbf{B}$, with T the time duration for proton to move to the axis under the radial electric field E_r . It explains a significant spin precession in the simulations. First, due to the small proton velocity, the precession time T in the magnetic fields is long; second, the anomalous magnetic moment G is larger than that of electrons; third, spin precession of a proton is directly affected by the trajectory and the field structure of the plasma channel, where the azimuthal magnetic field $B_\phi \sim 8m\omega/q$ in the plasma channel is strong.

The strong precession leads to a significant proton depolarization. Due to the cylindrical symmetry of the plasma channel, the transverse spin components, s_x and s_y , spread symmetrically. This concurs with the spin distribution on the Bloch sphere shown in Fig. 2(b). The polarization of the collected proton sample is thus determined by the longitudinal spin component $P = \langle s_z \rangle$. When the protons are focused to the axis, the longitudinal spin component of front protons around $z = z_f$ decreases to $s_z \sim 80\%$ as shown in Fig. 4(b). This indicates that the magnetic field is strong enough to significantly depolarize the accelerated beam protons. In the channel driven by lasers with $a_0 = 25$, about 80 % of the polarization is retained. For tail protons with further acceleration in the channel $z < z_f$ in Fig. 4(a), they conserve their momentum and continue to travel radially away after they cross the laser axis, which results in a change of the direction of B_ϕ . Figure 4(b) shows larger s_z of these protons indicating they precess back to their initial direction along z .

At the rear boundary of the gas jet, protons experience the second stage acceleration. When the front of the proton filament passes z_2 and enters the region with strong longitudinal electric field [see Figs. 3(c) and (d)], corresponding protons are accelerated intensely to 40 MeV [see

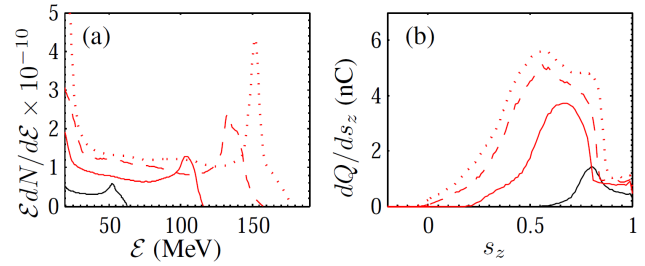


FIG. 5. Snapshots at $t = 330\lambda/c$ of: (a) Energy spectra and (b) spin distribution of accelerated protons with $\mathcal{E} \geq 20$ MeV in cases with $a_0 = 25, 50, 75$ and 100 , which are presented with solid-black, solid-red, dashed-red and dotted-red curves, respectively.

TABLE I. Polarized beams accelerated by PW lasers. Results from Fig. 5 are compared and the parameters used are given. Here, P_L is the laser power, \mathcal{E}_p the peak proton energy, Q the total charge, P the beam polarization.

a_0	P_L [PW]	\mathcal{E}_p [MeV]	Q [nC]	P [%]
25	1.34	53	0.26	82
50	5.37	105	1.3	65
75	12.1	133	2.4	57
100	21.5	152	3.1	56

Fig. 4(c)]. Meanwhile, the spin vector of front protons precesses roughly at the same rate ($\sim 80\%$) compared to the front protons in the plasma channel, see Figs. 4(b) and (d). Due to the limited lifetime of the strong accelerating field shown in Fig. 3(c), the tail protons in the filament will not be accelerated in the second acceleration stage. Figure 2(a) indicates that only the front protons in the filament are accelerated to an energy > 20 MeV. In other words, the tail protons neither contribute to the final accelerated proton beam nor to the beam polarization.

After the second-stage acceleration at the rear boundary of the gas jet, electromagnetic fields around the accelerated beam quickly decay. Thus both energy and polarization of the proton beam remains constant. Properties of the final accelerated proton beams with $\mathcal{E} \geq 20$ MeV are presented in Fig. 2 and solid-black lines in Fig. 5. Applying laser systems with a power of 1.3 PW, the protons are accelerated to tens of MeV with a peak at 53 MeV, while 82 % polarization is retained. The corresponding proton current shown in Fig. 2(a) is of the order of 10 kiloampere. Simulations with lower target density ($n_p \sim 10^{18} \text{ cm}^{-3}$) results in lower charge of the accelerated polarized proton beam (not shown). The accelerated energy and beam charge, as listed in Table I, increases with the driving laser intensity. A systematic study of other experimental parameters, like target density and length or the species of the halide atoms, on the proton energy distribution, flux and polarization is under way and will be subject of a forthcoming publica-

tion. More importantly, as shown in Fig. 5(b) and Table I, more than 50 % of the proton beam polarization driven by PW lasers can be sustained.

We would like to thank Z.Y.Li for helpful discussions. This work was supported by the Ministry of Science and Technology of the Peoples Republic of China (Grant Nos. 2018YFA0404803, 2016YFA0401102), the National Natural Science Foundation of China (Grant Nos. 11674339, 11922515, 11935008), the Strategic Priority Research Program of the Chinese Academy of Sciences (Grant No. XDB16) and Innovation Program of Shanghai Municipal Education Commission. The work of M.B. and A.H. has been carried out in the framework of the *JuSPARC* (Jülich Short-Pulse Particle and Radiation Center) and has been supported by the ATHENA (Accelerator Technology HElmholtz iNfrAstructure) consortium.

* wenmeng@hubu.edu.cn

† zhxm@siom.ac.cn

[1] T. R. Gentile, P. J. Nacher, B. Saam, and T. G. Walker, Optically polarized ^3He , *Rev. Mod. Phys.* **89**, 045004 (2017).

[2] M. S. Safranova, D. Budker, D. DeMille, D. F. J. Kimball, A. Derevianko, and C. W. Clark, Search for new physics with atoms and molecules, *Rev. Mod. Phys.* **90**, 025008 (2018).

[3] L. Adamczyk, J. K. Adkins, G. Agakishiev, M. M. Aggarwal, Z. Ahammed, I. Alekseev, A. Aparin, D. Arkhipkin, E. C. Aschenauer, A. Attri, *et al.* (STAR Collaboration), Measurement of the transverse single-spin asymmetry in $p + p \rightarrow W^\pm/Z^0$ at rhic, *Phys. Rev. Lett.* **116**, 132301 (2016).

[4] E. C. Aschenauer, S. Fazio, J. H. Lee, H. Mäntysaari, B. S. Page, B. Schenke, T. Ullrich, R. Venugopalan, and P. Zurita, The electronion collider: assessing the energy dependence of key measurements, *Rep. Prog. Phys.* **82**, 024301 (2019).

[5] D. de Florian, R. Sassot, M. Stratmann, and W. Vogelsang, Evidence for polarization of gluons in the proton, *Phys. Rev. Lett.* **113**, 012001 (2014).

[6] C. Alexandrou, M. Constantinou, K. Hadjyiannakou, K. Jansen, C. Kallidonis, G. Koutsou, A. V. Aviles-Casco, and C. Wiese, Nucleon spin and momentum decomposition using lattice qcd simulations, *Phys. Rev. Lett.* **119**, 142002 (2017).

[7] D. Androic *et al.* (The Jefferson Lab Qweak Collaboration), Precision measurement of the weak charge of the proton, *Nature* **557**, 207 (2018).

[8] A. Accardi, J. L. Albacete, M. Anselmino, N. Armesto, E. C. Aschenauer, A. Bacchetta, D. Boer, W. K. Brooks, T. Burton, N. B. Chang, *et al.*, Electron-ion collider: The next qcd frontier, *The European Physical Journal A* **52**, 268 (2016).

[9] S. R. Mane, Y. M. Shatunov, and K. Yokoya, Spin-polarized charged particle beams in high-energy accelerators, *Rep. Prog. Phys.* **68**, 1997 (2005).

[10] V. Yanovsky, V. Chvykov, G. Kalinchenko, P. Rousseau, T. Planchon, T. Matsuoka, A. Maksimchuk, J. Nees, G. Cheriaux, G. Mourou, *et al.*, Ultra-high intensity-300-TW laser at 0.1 Hz repetition rate., *Opt. Express* **16**, 2109 (2008).

[11] Z. Guo, L. Yu, J. Wang, C. Wang, Y. Liu, Z. Gan, W. Li, Y. Leng, X. Liang, and R. Li, Improvement of the focusing ability by double deformable mirrors for 10-PW-level Ti: sapphire chirped pulse amplification laser system, *Opt. Express* **26**, 26776 (2018).

[12] J. W. Yoon, C. Jeon, J. Shin, S. K. Lee, H. W. Lee, I. W. Choi, H. T. Kim, J. H. Sung, and C. H. Nam, Achieving the laser intensity of $5.5 \times 10^{22} \text{ W/cm}^2$ with a wavefront-corrected multi-PW laser, *Opt. Express* **27**, 20412 (2019).

[13] F. Wagner, O. Deppert, C. Brabetz, P. Fiala, A. Kleinschmidt, P. Poth, V. A. Schanz, A. Tebartz, B. Zielbauer, M. Roth, *et al.*, Maximum proton energy above 85 mev from the relativistic interaction of laser pulses with micrometer thick ch_2 targets, *Phys. Rev. Lett.* **116**, 205002 (2016).

[14] I. J. Kim, K. H. Pae, I. W. Choi, C.-L. Lee, H. T. Kim, H. Singhal, J. H. Sung, S. K. Lee, H. W. Lee, P. V. Nickles, *et al.*, Radiation pressure acceleration of protons to 93MeV with circularly polarized petawatt laser pulses, *Physics of Plasmas* **23**, 070701 (2016).

[15] H. Zhang, B. F. Shen, W. P. Wang, S. H. Zhai, S. S. Li, X. M. Lu, J. F. Li, R. J. Xu, X. L. Wang, X. Y. Liang, *et al.*, Collisionless shock acceleration of high-flux quasi-monoenergetic proton beams driven by circularly polarized laser pulses, *Phys. Rev. Lett.* **119**, 164801 (2017).

[16] P. Hilz, T. M. Ostermayr, A. Huebl, V. Bagnoud, B. Borm, M. Bussmann, M. Gallei, J. Gebhard, D. Haffa, J. Hartmann, *et al.*, Isolated proton bunch acceleration by a petawatt laser pulse, *Nature Communications* **9**, 423 (2018).

[17] W. J. Ma, I. J. Kim, J. Q. Yu, I. W. Choi, P. K. Singh, H. W. Lee, J. H. Sung, S. K. Lee, C. Lin, Q. Liao, *et al.*, Laser acceleration of highly energetic carbon ions using a double-layer target composed of slightly underdense plasma and ultrathin foil, *Phys. Rev. Lett.* **122**, 014803 (2019).

[18] S. D. Kraft, L. Obst, J. Metzkes-Ng, H.-P. Schlenvoigt, K. Zeil, S. Michaux, D. Chatain, J.-P. Perin, S. N. Chen, J. Fuchs, M. Gauthier, T. E. Cowan, and U. Schramm, First demonstration of multi-MeV proton acceleration from a cryogenic hydrogen ribbon target, *Plasma Physics and Controlled Fusion* **60**, 044010 (2018).

[19] F. A. Asenjo, J. Zamanian, M. Marklund, G. Brodin, and P. Johansson, Semi-relativistic effects in spin-1/2 quantum plasmas, *New Journal of Physics* **14**, 073042 (2012).

[20] T.-O. Müller and C. Müller, Longitudinal spin polarization in multiphoton bethe-heitler pair production, *Phys. Rev. A* **86**, 022109 (2012).

[21] M. Wen, H. Bauke, and C. H. Keitel, Identifying the Stern-Gerlach force of classical electron dynamics, *Sci. Rep.* **6**, 31624 (2016).

[22] M. Wen, C. H. Keitel, and H. Bauke, Spin-one-half particles in strong electromagnetic fields: Spin effects and radiation reaction, *Phys. Rev. A* **95**, 042102 (2017).

[23] N. Raab, M. Büscher, M. Cerchez, R. Engels, I. Engin, P. Gibbon, P. Greven, A. Holler, A. Karmakar, A. Lehrach, R. Maier, M. Swantusch, M. Toncian, T. Toncian, and O. Willi, Polarization measurement of laser-accelerated protons, *Physics of Plasmas* (1994-present) **21**, 023104 (2014).

[24] D. D. Sorbo, D. Seipt, A. G. R. Thomas, and C. P. Ridgers, Electron spin polarization in realistic trajectories around the magnetic node of two counter-propagating, circularly polarized, ultra-intense lasers, *Plasma Physics and Controlled Fusion* **60**, 064003 (2018).

[25] H.-H. Song, W.-M. Wang, J.-X. Li, Y.-F. Li, and Y.-T. Li, Spin-polarization effects of an ultrarelativistic electron beam in an ultraintense two-color laser pulse, *Phys. Rev. A* **100**, 033407 (2019).

[26] A. Hützen, J. Thomas, J. Böker, R. Engels, R. Gebel, A. Lehrach, A. Pukhov, T. P. Rakitzis, D. Sofikitis, M. Büscher, and et al., Polarized proton beams from laser-induced plasmas, *High Power Laser Science and Engineering* **7**, e16 (2019).

[27] M. Büscher, A. Hützen, I. Engin, J. Thomas, A. Pukhov, J. Böker, R. Gebel, A. Lehrach, R. Engels, T. Peter Rakitzis, and D. Sofikitis, Polarized proton beams from a laser-plasma accelerator, *International Journal of Modern Physics A* , 1942028 (2019).

[28] Y.-F. Li, R. Shaisultanov, K. Z. Hatsagortsyan, F. Wan, C. H. Keitel, and J.-X. Li, Ultrarelativistic electron-beam polarization in single-shot interaction with an ultraintense laser pulse, *Phys. Rev. Lett.* **122**, 154801 (2019).

[29] M. Wen, M. Tamburini, and C. H. Keitel, Polarized laser-wakefield-accelerated kiloampere electron beams, *Phys. Rev. Lett.* **122**, 214801 (2019).

[30] Y. Wu, L. Ji, X. Geng, Q. Yu, N. Wang, B. Feng, Z. Guo, W. Wang, C. Qin, X. Yan, L. Zhang, J. Thomas, A. Hützen, A. Pukhov, M. Büscher, B. Shen, and R. Li, Polarized electron acceleration in beam-driven plasma wakefield based on density down-ramp injection, *Phys. Rev. E* **100**, 043202 (2019).

[31] J. Thomas, A. Hützen, A. Lehrach, A. Pukhov, L. Ji, Y. Wu, X. Geng, and M. Büscher, Scaling laws for the (de-)polarization time of relativistic particle beams in strong fields, *arXiv:2001.07084* (2020).

[32] D. Sofikitis, C. S. Kannis, G. K. Boulogiannis, and T. P. Rakitzis, Ultrahigh-Density Spin-Polarized H and D Observed via Magnetization Quantum Beats, *Phys. Rev. Lett.* **121**, 083001 (2018).

[33] L. Willingale, S. P. D. Mangles, P. M. Nilson, R. J. Clarke, A. E. Dangor, M. C. Kaluza, S. Karsch, K. L. Lancaster, W. B. Mori, Z. Najmudin, J. Schreiber, A. G. R. Thomas, M. S. Wei, and K. Krushelnick, Collimated multi-mev ion beams from high-intensity laser interactions with underdense plasma, *Phys. Rev. Lett.* **96**, 245002 (2006).

[34] B. Shen, Y. Li, M. Y. Yu, and J. Cary, Bubble regime for ion acceleration in a laser-driven plasma, *Phys. Rev. E* **76**, 055402 (2007).

[35] X. Zhang, B. Shen, L. Zhang, J. Xu, X. Wang, W. Wang, L. Yi, and Y. Shi, Proton acceleration in underdense plasma by ultraintense laguerre-gaussian laser pulse, *New Journal of Physics* **16**, 123051 (2014).

[36] B. Liu, J. Meyer-ter Vehn, and H. Ruhl, Self-trapping and acceleration of ions in laser-driven relativistically transparent plasma, *Physics of Plasmas* **25**, 103117 (2018).

[37] I. Engin, Z. M. Chitgar, O. Deppert, L. D. Lucchio, R. Engels, P. Fedorets, S. Frydrych, P. Gibbon, A. Klein-schmidt, A. Lehrach, R. Maier, D. Prasuhn, M. Roth, F. Schlter, C. M. Schneider, T. Sthlker, K. Strathmann, and M. Bscher, Laser-induced acceleration of helium ions from unpolarized gas jets, *Plasma Physics and Controlled Fusion* **61**, 115012 (2019).

[38] T. D. Arber, K. Bennett, C. S. Brady, A. Lawrence-Douglas, M. G. Ramsay, N. J. Sircombe, P. Gillies, R. G. Evans, H. Schmitz, A. R. Bell, et al., Contemporary particle-in-cell approach to laser-plasma modelling, *Plasma Phys. Contr. F.* **57**, 113001 (2015).

[39] L. D. Landau and E. M. Lifshitz, *The Classical Theory of Fields* (Butterworth-Heinemann, Oxford, 1980).

[40] S. Semushin and V. Malka, High density gas jet nozzle design for laser target production, *Review of Scientific Instruments* **72**, 2961 (2001).

[41] K. Schmid and L. Veisz, Supersonic gas jets for laser-plasma experiments, *Review of Scientific Instruments* **83**, 053304 (2012).

[42] S. Lorenz, G. Grittani, E. Chacon-Golcher, C. M. Lazarini, J. Limpouch, F. Nawaz, M. Nevrkla, L. Vilanova, and T. Levato, Characterization of supersonic and subsonic gas targets for laser wakefield electron acceleration experiments, *Matter and Radiation at Extremes* **4**, 015401 (2019).

[43] K. I. Popov, W. Rozmus, V. Y. Bychenkov, N. Naseri, C. E. Capjack, and A. V. Brantov, Ion response to relativistic electron bunches in the blowout regime of laser-plasma accelerators, *Phys. Rev. Lett.* **105**, 195002 (2010).

[44] L. L. Ji, A. Pukhov, I. Y. Kostyukov, B. F. Shen, and K. Akli, Radiation-reaction trapping of electrons in extreme laser fields, *Phys. Rev. Lett.* **112**, 145003 (2014).

[45] T. Nakamura, S. V. Bulanov, T. Z. Esirkepov, and M. Kando, High-energy ions from near-critical density plasmas via magnetic vortex acceleration, *Phys. Rev. Lett.* **105**, 135002 (2010).

[46] S. Kawata, T. Nagashima, M. Takano, T. Izumiya, D. Kamiyama, D. Barada, Q. Kong, Y. J. Gu, P. X. Wang, Y. Y. Ma, and et al., Controllability of intense-laser ion acceleration, *High Power Laser Science and Engineering* **2**, e4 (2014).

[47] J. Park, S. S. Bulanov, J. Bin, Q. Ji, S. Steinke, J.-L. Vay, C. G. R. Geddes, C. B. Schroeder, W. P. Leemans, T. Schenkel, and E. Esarey, Ion acceleration in laser generated megatesla magnetic vortex, *Physics of Plasmas* **26**, 103108 (2019).

[48] L. H. Thomas, The motion of the spinning electron, *Nature* **117**, 514 (1926).

[49] V. Bargmann, V. L. Telegdi, and L. Michel, Precession of the polarization of particles moving in a homogeneous electromagnetic field, *Phys. Rev. Lett.* **2**, 435 (1959).